Mechanical and electrical response due to fluid-pressure equilibration following an earthquake

Steven R. Pride,[1] Frédérique Moreau, and Pierre Gavrilenko
Équipe de Géophysique, Géosciences Rennes, Université de Rennes 1, Rennes, France

Received 15 July 2003; revised 9 January 2004; accepted 16 January 2004; published 9 March 2004.

[1] The mechanical and electrical response in a uniform porous crust are determined following a shear dislocation (earthquake) on an internal slip surface. A uniform crust is studied because many exact analytical relations hold between the various response fields in this case. The initial stress field that is created immediately following the earthquake subsequently relaxes through time as the fluid pressure equilibrates by fluid flow. Maps of the electric field generated due to the fluid flow (electrokinetic coupling) are presented. Using conservative estimates of the various parameters involved, electric fields significantly larger than the diurnal (magnetotelluric) fields are generated. Quantitative results for how various components of the stress tensor change due to the fluid equilibration are also presented. The Coulomb stress can easily change by 100% (and more) in the months following an earthquake due to the fluid-pressure equilibration. *INDEX TERMS:* 7212 Seismology: Earthquake ground motions and engineering; 5104 Physical Properties of Rocks: Fracture and flow; 5114 Physical Properties of Rocks: Permeability and porosity; 8164 Tectonophysics: Stresses—crust and lithosphere; *KEYWORDS:* earthquake, poroelasticity, electrokinetic

Citation: Pride, S. R., F. Moreau, and P. Gavrilenko (2004), Mechanical and electrical response due to fluid-pressure equilibration following an earthquake, *J. Geophys. Res.*, *109*, B03302, doi:10.1029/2003JB002690.

1. Introduction

[2] An earthquake creates lobes of compression and dilation in the crust surrounding the fault segment that slipped. Within these lobes, the changes in tangential and normal stress on potential slip surfaces may either promote or hinder the arrival of aftershocks. As reviewed, for example, by *Stein* [1999], such mainshock-induced Coulomb-stress changes are one of the few predictive mechanisms known to trigger earthquakes. However, the reason for the time delay between when a mainshock occurs and when the aftershocks occur is not entirely understood.

[3] One possibility initially suggested by *Nur and Booker* [1972] is that the delay is caused by fluid-pressure diffusion from the lobes of compression to the lobes of dilation. As fluid pressure slowly increases in a dilated region due to diffusion, it acts to further increase the Coulomb-stress change in that region and may trigger an aftershock weeks or months after the main event.

[4] P. Gavrilenko (Hydromechanical coupling in response to earthquakes: On the possible consequences for aftershocks, submitted to *Geophysical Journal International*, 2004) (hereinafter referred to as Gavrilenko, submitted manuscript, 2004) has recently numerically modeled the fluid-pressure redistribution in a uniform crust following an earthquake. He determines the aftershock sequence triggered by Coulomb-stress changes when fluid-pressure diffusion alone is responsible for the time delays and has shown that much about the aftershock sequence of real earthquakes can be described in this way. Among other things, he observes a fall off in the rate $\Delta N/\Delta t$ of aftershock occurrence that is consistent with a dimensionless Omori's law in the form $t_d \Delta N/\Delta t \propto (\epsilon + t/t_d)^{-p}$ where $\Delta N(t)$ are the number of aftershocks occurring in each time increment Δt a time t after the mainshock. The diffusive time scale t_d is given by $t_d = \ell^2/D$ where ℓ is an equilibration length that measures distance between the static-stress lobes and D is the fluid-pressure diffusivity. The exponent p is generally near 1 but seemingly has a slight dependence on fault geometry and the assumed slip function for the mainshock. The tiny positive constant ϵ satisfies $\epsilon \ll 1$ and accounts for an initially more modest seismicity decay in the early hours following the mainshock.

[5] Our goal in the present paper is not to study aftershock sequences per se, but to carefully study the nature of the mechanical and electrical response induced in a uniform crust by a mainshock. The mainshock is modeled as a shear dislocation on an internal slip surface, and the *Okada* [1992] program is used to numerically determine the stress distribution at $t = 0$. The focus of the paper is on how the various fields decay through time throughout the crust due to fluid-pressure equilibration. Gavrilenko (submitted manuscript, 2004) did not allow for the stress tensor to evolve through time due to diffusion and we allow for this poroelastic effect here. In a uniform crust, many exact things can be analytically stated about the nature of such poroelastic response. Although the earth's crust is far from being homogeneous,

[1] Now at Earth Sciences Division, Lawrence Berkeley National Laboratory, Berkeley, California, USA.

0148-0227/04/2003JB002690$09.00

we nonetheless feel that the uniform half-space model has considerable pedagogic value and can be used as a benchmark for more numerically intensive models.

[6] The coupling mechanism that generates the electric fields (E fields) is electrokinetic in nature. It is shown that using conservative values for the electrokinetic parameters, E fields after an $M6$ event can have amplitudes 100 times larger than the diurnal E fields that are generated each day as the sun heats the ionosphere (and that are routinely measured during magnetotelluric surveys). The E fields decay with the same time constant t_d as the fluid-pressure equilibration. By measuring the E fields through time, it should be possible to discern the fluid-pressure diffusivity of the crust at the scale ℓ of the static compressional lobes.

[7] Previous work that modeled E fields due to electrokinetic processes associated with earthquakes has either focused on the possible flow within the fault zone [e.g., *Fenoglio et al.*, 1995] or on precursory flow associated with the possible creation of idealized dilatant zones prior to an earthquake [e.g., *Fitterman*, 1978]. No previous study, to our knowledge, has ever focused on the E fields (or stress-tensor variations) generated by the static-stress changes and subsequent fluid-pressure diffusion throughout the crust due to slip on a fault surface. The present study suggests that by monitoring the electrical field through time (e.g., in a network of monitoring wells), information about the crustal scale fluid-pressure equilibration following a mainshock can be discerned.

2. Governing Equations

[8] The governing equations for this problem are the laws of poroelasticy [e.g., *Biot*, 1962] coupled with the laws of electrostatics with the electrokinetic coupling occurring in the transport equations. The following equations correspond to the quasi-static limit of those established by *Pride* [1994]:

$$\nabla \cdot \boldsymbol{\tau}^D = \nabla P_c \tag{1}$$

$$\boldsymbol{\tau}^D = G\left(\nabla \mathbf{u} + \nabla \mathbf{u}^T - \frac{2}{3}\nabla \cdot \mathbf{u}\mathbf{I}\right) \tag{2}$$

$$-\begin{bmatrix} P_c \\ p_f \end{bmatrix} = K_U \begin{bmatrix} 1 & B \\ B & B/\alpha \end{bmatrix} \begin{bmatrix} \nabla \cdot \mathbf{u} \\ \nabla \cdot \mathbf{w} \end{bmatrix} \tag{3}$$

$$\frac{\partial \mathbf{w}}{\partial t} = -\frac{k}{\eta}\nabla p_f + L\mathbf{E} \tag{4}$$

$$\mathbf{J} = -L\nabla p_f + \sigma \mathbf{E} \tag{5}$$

$$\nabla \times \mathbf{H} = \mathbf{J} \tag{6}$$

$$\nabla \times \mathbf{E} = 0. \tag{7}$$

In the present study, the response fields in these equations are all created by an earthquake and are: the deviatoric stress tensor $\boldsymbol{\tau}^D$, the confining pressure P_c, the fluid pressure p_f, the solid displacements $\mathbf{u}$, the fluid-filtration displacement $\mathbf{w}$ (defined so that $\partial \mathbf{w}/\partial t$ is the Darcy velocity), the electric current density $\mathbf{J}$, the electric field $\mathbf{E}$, and the magnetic field $\mathbf{H}$. Upon taking a time derivative of the compressibility law (3), the filtration displacement $\mathbf{w}$ can be replaced everywhere by the Darcy flux $\mathbf{q} = \partial \mathbf{w}/\partial t$ if so desired.

[9] The three poroelastic constants are the undrained bulk modulus K_U (confining-pressure change divided by dilatation for a sealed sample of the porous material), *Skempton*'s [1954] coefficient B (fluid-pressure change divided by confining-pressure change for a sealed sample), and the *Biot and Willis* [1957] constant α that is defined

$$\alpha = (1 - K_D/K_U)/B \tag{8}$$

where K_D is the drained bulk modulus (confining-pressure change divided by dilatation under conditions where the fluid pressure does not change). The Biot-Willis constant α is entirely independent of the fluid in the pores even though B and K_U both depend on the fluid bulk modulus [e.g., *Berge et al.*, 1993]. The remaining material properties are the shear modulus G, the rock permeability k, the fluid viscosity η, the rock's electrical conductivity σ, and the electrokinetic-coupling coefficient L. Models for these various coefficients/material-properties are given and discussed in Appendix A.

[10] The electrokinetic coupling in equation (5) by which a fluid-pressure gradient drives an electric current is called "electro-filtration". The coupling in equation (4) by which an electric field drives a fluid flow is called "electro-osmosis" and is of second-order importance in the present study. These phenomena are both due to the presence of a charge separation (the double layer) present at the interface between water and solid surfaces such as silicate grains in rocks. A layer of charged surface sites and/or adsorbed ions on the grain surfaces is balanced by a diffuse layer of oppositely charged free ions in the liquid immediately adjacent to the grain surfaces. In electrofiltration, an applied fluid-pressure gradient transports the water and free ions of the diffuse layer relative to the fixed charge of the adsorbed layer resulting in an electric current called the "streaming current". In electro-osmosis, an applied E field acts as a body force on the diffuse layer charge resulting in fluid flow.

[11] The use of the electrostatic equations (6) and (7) is now justified. The displacement current $\partial \mathbf{D}/\partial t$ in the complete Ampére's law $\nabla \times \mathbf{H} = \mathbf{J} + \partial \mathbf{D}/\partial t$ may be neglected relative to $\mathbf{J}$ when the temporal frequencies f satisfy $f \ll \sigma/(2\pi\varepsilon)$ where σ is the electrical conductivity and ϵ the electrical permittivity of the material. Throughout the crust, we generally have $\sigma/(2\pi\varepsilon) > 10^6$ Hz while the frequency content of the fluid-pressure diffusion that is creating the electric field is generally in the range $f < 10^{-2}$ Hz. The displacement current may therefore be neglected. Further, at these low frequencies, the electromagnetic skin depth $\delta = 1/\sqrt{2\pi\mu_o\sigma f}$ (where μ_o is the magnetic permeability of vacuum) extends well into the mantle so that the entire crust can be considered as lying within the electrostatic near field. Accordingly, induction effects can be entirely neglected and Faraday's law becomes $\nabla \times \mathbf{E} = -\partial \mathbf{B}/\partial t = 0$ throughout the crust.

[12] Last, the boundary conditions that hold over the earth's surface $z = 0$ are that: (1) the stress change generated by an earthquake produces no stress change in the atmosphere; (2) the fluid may escape freely through the unsealed surface of the earth (so-called "open-pore" boundary conditions); and, (3) since electrostatic equilibrium always holds, the normal component of the electrical-current density must be zero at the surface. In mathematical terms, these three boundary conditions are expressed

$$\hat{\mathbf{z}} \cdot \left(\boldsymbol{\tau}^D - P_c \mathbf{I}\right) = 0, \quad p_f = 0, \quad \text{and} \quad \hat{\mathbf{z}} \cdot \mathbf{J} = 0. \tag{9}$$

Further, all fields approach zero at infinite distance from the earthquake source. The source for the problem is a prescribed amount of shear dislocation on an internal fault surface. If for some reason it is desired to treat the earth's surface as being sealed to flow, the second two conditions are replaced with $\partial p_f/\partial z = 0$ and $\mathbf{z} \cdot \mathbf{E} = 0$ respectively; i.e., the z-components of equations (4) and (5) must both be zero at the surface.

3. Response in a Uniform Half-Space

[13] If analysis is restricted to a uniform crustal model, many exact things can be determined about the nature of the earthquake response as is now developed over the following subsections.

3.1. Electric and Magnetic Response

[14] Faraday's law (7) is satisfied by introducing an electric potential $\mathbf{E} = -\nabla\varphi$. Taking the divergence of Ampére's law (6) gives $\nabla \cdot \mathbf{J} = 0$ so that upon introducing the generalized Ohm's law (5), the electric potential in a uniform crust exactly satisfies the boundary value problem

$$\nabla^2\varphi = -\frac{L}{\sigma}\nabla^2 p_f \tag{10}$$

subject to the insulating surface condition that $\hat{\mathbf{z}} \cdot \mathbf{J} = 0$ or

$$\partial\varphi/\partial z = -(L/\sigma)\partial p_f/\partial z \tag{11}$$

on $z = 0$. Thus we have the simple result that in a uniform crust (and only in a uniform crust) the electric potential is given by

$$\varphi(\mathbf{r}, t) = -\frac{L}{\sigma} p_f(\mathbf{r}, t). \tag{12}$$

Because of this fact, $\mathbf{J} = 0$ everywhere and there are no magnetic fields generated. Upon taking the gradient of equation (12) and using the generalized Darcy law (4), the electric field is found to be directly proportional to the local filtration velocity:

$$\mathbf{E} = -\frac{L\eta}{k\sigma}\left(1 - \frac{\eta L^2}{k\sigma}\right)^{-1}\frac{\partial \mathbf{w}}{\partial t} \tag{13}$$

where the L^2 correction corresponds to a second-order electro-osmotic feed back and can be neglected; however, we retain it for completeness.

[15] Because $p_f = 0$ everywhere on an unsealed surface, both (12) and (13) tell us that no horizontal components to the electric field are present along the unsealed surface of a uniform crustal half-space. However, there will be a significant vertical component to the E field along the surface (so that the normal component of the electrical current density is zero). For there to be either horizontal components of an E field or magnetic fields present at the unsealed surface, heterogeneity is required.

[16] Note that if the surface were taken to be sealed to flow, then equation (12) would again hold but because p_f will now have lateral variations along the surface, we will have that $\hat{\mathbf{z}} \times \nabla\varphi \times \hat{\mathbf{z}} \neq 0$ and thus horizontal electrical fields would be present on $z = 0$. *Sill* [1983] promoted such sealed conditions because it seemed inappropriate to him to have water emerge from the earth at the surface. Although confined aquifers do exist in which the top surface is sealed and the charging and discharging occur principally in the horizontal direction, they are three-dimensional objects outside the scope of the present study. It is now a well-documented fact [e.g., *Muir-Wood and King*, 1993] that stream flow can increase at the earth's surface following an earthquake and although the precise modeling of a moving water table is certainly a point for ongoing research, the open-pore boundary condition $p_f = 0$ at the earth's surface is appropriate in the present study concerned with a uniform crust.

3.2. Poroelastic Response

[17] In a uniform material, the poroelastic response formally decomposes into two independent modes as is most conveniently seen upon taking the spatial Fourier transform of equations (1)–(7) [cf. *Pride*, 2004]. In one mode, the fluid accumulations $\nabla \cdot \mathbf{w}$ are exactly zero and the response is completely undrained. The other mode corresponds to a pure fluid-pressure diffusion.

3.2.1. Undrained Response

[18] Introducing $\nabla \cdot \mathbf{w} = 0$ into the poroelastic governing equations (1)–(3) produces the standard elasto-static equation

$$(K_U + G/3)\nabla\nabla \cdot \mathbf{u} + G\nabla^2\mathbf{u} = 0. \tag{14}$$

If an inertial force $\rho\partial^2\mathbf{u}/\partial t^2$ had been included on the right-hand side, this mode would correspond to the fast-P and S wave response in the low-frequency limit of Biot's theory. However, our interest here is not with the transient effects associated with waves produced by the earthquake and so we have neglected all inertial effects from the outset.

[19] This time-independent undrained mode is excited in the present problem by a prescribed amount of slip on an internal dislocation surface (the fault). To calculate the undrained displacement response $\mathbf{u}(\mathbf{r})$, equation (14) is solved subject to the free surface condition $\hat{\mathbf{z}} \cdot [G(\nabla\mathbf{u} + \nabla\mathbf{u}^T) + (K_U - 2G/3)\nabla \cdot \mathbf{u}\mathbf{I}] = 0$ on $z = 0$ and subject to the internal dislocation. This problem is solved here using the now standard [*Okada*, 1992] numerical program. The undrained ($t = 0$) fluid pressure distribution may then be determined everywhere throughout $z > 0$ using $-p_f(\mathbf{r}, 0) = K_U B\nabla \cdot \mathbf{u}(\mathbf{r}) = -BP_c(\mathbf{r})$.

3.2.2. Fluid-Pressure Variations

[20] The other poroelastic response corresponds to the *Biot* [1956] slow wave which, at the low-frequencies considered here, corresponds to a pure fluid-pressure diffusion as is now demonstrated.

[21] In a uniform material, the fluid accumulations and volume dilatations in the slow wave are exactly related as [e.g., *Pride*, 2004; *Pride and Haartsen*, 1996]

$$\nabla \cdot \mathbf{w} = \beta \nabla \cdot \delta\mathbf{u} \tag{15}$$

where the total displacement field is being decomposed into a static-undrained and diffusive contribution as $\mathbf{u}^{\text{tot}}(\mathbf{r}, t) = \mathbf{u}(\mathbf{r}) + \delta\mathbf{u}(\mathbf{r}, t)$. Taking the low-frequency limit of the β obtained by *Pride and Haartsen* [1996] gives

$$\beta = -\frac{1}{B}\left(1 + \frac{4G}{3K_U}\right) \tag{16}$$

which is rigorously independent of the electrokinetic coupling coefficient L. The presence of the shear modulus is because the slow wave (fluid-pressure-diffusion front) is a uniaxial longitudinal deformation with displacements perpendicular to the front and no displacements parallel with the front. Fluid-pressure diffusion in porous media therefore has a shear component associated with it and is not a purely dilatational phenomena.

[22] Taking the time derivative of equation (3) and the divergence of equation (4) and introducing equations (10), (15), and (16), gives the diffusion equation

$$D\nabla^2 p_f - \frac{\partial p_f}{\partial t} = 0 \tag{17}$$

with the fluid-pressure diffusivity D given exactly by

$$D = \frac{k}{\eta}\frac{BK_U}{\alpha}\left(\frac{K_D + 4G/3}{K_U + 4G/3}\right)\left(1 - \frac{\eta L^2}{\sigma k}\right). \tag{18}$$

The $O(L^2)$ electrokinetic correction, that is a result of the created E field retarding fluid flow, is always entirely negligible; however, we retain it for completeness.

[23] The approach for determining the $t > 0$ slow-wave response is to first solve for the fluid pressure using equation (17) along with the initial data $p_f(\mathbf{r}, 0) = BP_c(\mathbf{r})$ determined from the undrained response and with the free surface condition $p_f = 0$ on $z = 0$. Note that the free-surface condition for the undrained response is that $\hat{\mathbf{z}} \cdot \boldsymbol{\tau}^D = P_c\hat{\mathbf{z}}$ and may correspond to having $P_c \neq 0$. on the surface. Thus, in addition to the diffusion between the lobes at depth surrounding the fault limits there is an additional (but typically much weaker) diffusion that begins at the surface and progresses downward into the crust so that $p_f = 0$ on $z = 0$ is always satisfied for all $t > 0$.

[24] Given the fluid-pressure variation through time, it is straightforward to calculate how the displacements and confining pressures are modified through time due to the fluid-pressure diffusion. The following results are given principally for anyone wishing to model how Coulomb stress evolves through time due to fluid-pressure diffusion.

3.2.3. Confining-Pressure Variations

[25] First, we decompose the total confining pressure variation into an undrained-static change and a diffusive contribution; i.e., $P_c{}^{\text{tot}}(\mathbf{r}, t) = P_c(\mathbf{r}) + \delta p_c(\mathbf{r}, t)$ where, once again, the response $P_c(\mathbf{r})$ is determined at $t = 0$ using the *Okada* [1992] program. From equations (3), (15), and (16), the diffusive confining pressure changes are given by

$$\delta p_c(\mathbf{r}, t) = -\frac{\alpha B 4G/3}{K_D + 4G/3}\left[P_c(\mathbf{r}) - \frac{p_f(\mathbf{r}, t)}{B}\right]. \tag{19}$$

In a calculation of Coulomb stress, one needs the total effective pressure $P_e = P_c^{\text{tot}} - p_f$ which is then given by

$$P_e(\mathbf{r}, t) = P_c(\mathbf{r}) - p_f(\mathbf{r}, t) - \frac{\alpha B 4G/3}{K_D + 4G/3}\left[P_c(\mathbf{r}) - \frac{p_f(\mathbf{r}, t)}{B}\right]. \tag{20}$$

The Biot-Willis constant satisfies the thermodynamic stability constraint that $0 < \alpha < 1/B$. For water-saturated low-porosity laboratory samples of crustal rock, we typically have $0.1 < \alpha < B < 0.5$. Expressions for α and B that detail the parameters on which they depend are given in Appendix A (generally, the greater the consolidation, the smaller the values of either B or α). However, we recognize that the values of α and β appropriate for kilometer-scale samples of a fractally faulted crust is rather uncertain. The presence of joints or faults in a porous sample will enhance the values of α and B relative to the same sample without such joints.

[26] The total change in effective pressure due to fluid-pressure equilibration following an earthquake is then

$$\frac{P_e(\mathbf{r}, \infty) - P_e(\mathbf{r}, 0)}{P_e(\mathbf{r}, 0)} = \frac{B}{1 - B}\left(1 - \frac{\alpha 4G/3}{K_D + 4G/3}\right). \tag{21}$$

For $B = 0.5$, there is roughly a 100% change in the effective pressure due to diffusion while if $B = 0.75$ there is as much as a 300% change (more negative in the lobes that were initially negative and more positive in the lobes that were initially positive). Such large enhancements in Coulomb-stress demonstrates that diffusion can be responsible for considerable induced seismicity.

3.2.4. Deviatoric-Stress Variations

[27] To determine how the deviatoric stress tensor $\boldsymbol{\tau}^D$ evolves due to the fluid-pressure diffusion, we again decompose the total displacement field into static and diffusive contributions $\mathbf{u}^{\text{tot}}(\mathbf{r}, t) = \mathbf{u}(\mathbf{r}) + \delta\mathbf{u}(\mathbf{r}, t)$.

[28] Using $\nabla \cdot \mathbf{w} = \beta\nabla \cdot \delta\mathbf{u}$ in (3) gives the slow-wave result that $\delta p_c = 4G\nabla \cdot \delta\mathbf{u}/3$. Using this result in equations (1) and (2) then gives that the diffusive perturbations in the displacements obey $\nabla^2\,\delta\mathbf{u} - \nabla\nabla \cdot \delta\mathbf{u} = 0$ or

$$\nabla^2\delta\mathbf{u}(\mathbf{r}, t) = \frac{\alpha B}{(K_D + 4G/3)}\nabla\left[P_c(\mathbf{r}) - \frac{p_f(\mathbf{r}, t)}{B}\right]. \tag{22}$$

The stress-free surface condition for these displacements is that $\hat{\mathbf{z}} \cdot \nabla\delta\mathbf{u} + \nabla\delta\mathbf{u} \cdot \hat{\mathbf{z}} = 2\,(\nabla \cdot \delta\mathbf{u})\,\hat{\mathbf{z}}$ on $z = 0$ which can be written out component by component as

$$\frac{\partial \delta u_z}{\partial z} = \frac{\alpha B\, P_c(x, y, 0)}{K_D + 4G/3} \tag{23}$$

$$\frac{\partial \delta u_x}{\partial z} = -\frac{\partial \delta u_z}{\partial x} \tag{24}$$

$$\frac{\partial \delta u_y}{\partial z} = -\frac{\partial \delta u_z}{\partial y}. \tag{25}$$

Thus the Poisson problem for determining δu_z is decoupled from δu_x and δu_y. One first determines δu_z, and then uses the result to determine both δu_x and δu_y.

[29] We note in passing that *Bell and Nur* [1978] postulate $\nabla \times \delta\mathbf{u} = 0$ so that $\delta\mathbf{u} = -\nabla\Phi$ where Φ is a potential that satisfies a Poisson equation easily determined from equation (22). The longitudinal response will indeed be rotation free in an infinite whole space; however, it seems impossible to satisfy the free-surface condition with such a rotation-free displacement field. Upon inserting $\delta\mathbf{u} = -\nabla\Phi$ into the exact free-surface conditions (23)–(25), one obtains boundary conditions involving the second spatial derivatives of Φ. It is well-known that unique solutions to the Poisson problem must employ boundary conditions involving only the zeroth or first normal derivative of Φ. As such, we recommend a direct solution of $\delta\mathbf{u}$ using equations (22)–(25).

[30] One approach for determining δu_z is to introduce a Green function satisfying

$$\nabla^2 g = \delta(\mathbf{r} - \mathbf{r}_o) \text{ throughout } z \geq 0 \tag{26}$$

$$\frac{\partial g}{\partial z} = 0 \quad \text{on} \quad z = 0. \tag{27}$$

Carrying out the usual self-adjoint operations (multiply the z-component of (22) by g and multiply (26) by δu_z, subtract, integrate over the crustal half-space, use the divergence theorem, and apply the boundary conditions) gives

$$\frac{(K_D + 4G/3)}{\alpha B}\delta u_z(\mathbf{r}, t) = \int_{z=0} dS_o\, g(\mathbf{r}; \mathbf{r}_o) P_c(\mathbf{r}_o) + \int_{z\geq 0} dV_o\, g(\mathbf{r}; \mathbf{r}_o) \frac{\partial \left[P_c(\mathbf{r}_o) - p_f(\mathbf{r_o}, \mathbf{t})/B\right]}{\partial z_o}. \tag{28}$$

If the volume integral over $z \geq 0$ is integrated by parts and the divergence theorem again applied (note that the outward normal to $z = 0$ is $-\hat{\mathbf{z}}$ and that $p_f = 0$ on $z = 0$) one then obtains that

$$\delta u_z(\mathbf{r}, t) = \frac{\alpha B}{(K_D + 4G/3)} \int_{z\geq 0} dV_o \left[P_c(\mathbf{r}_o) - \frac{p_f(\mathbf{r_o}, \mathbf{t})}{B}\right] \frac{\partial g(\mathbf{r}; \mathbf{r}_o)}{\partial z_o}. \tag{29}$$

The Green function satisfying (26) and (27) is

$$g(\mathbf{r}; \mathbf{r}_o) = \frac{1}{4\pi}\left[\frac{1}{\sqrt{(x - x_o)^2 + (y - y_o)^2 + (z - z_o)^2}} + \frac{1}{\sqrt{(x - x_o)^2 + (y - y_o)^2 + (z + z_o)^2}}\right]. \tag{30}$$

In particular, the strain component $\partial\delta u_z/\partial y$ studied in the numerical section is given by

$$\frac{\partial \delta u_z(\mathbf{r}, t)}{\partial y} = \frac{\alpha B}{(K_D + 4G/3)} \int_{z\geq 0} dV_o \left[P_c(\mathbf{r}_o) - \frac{p_f(\mathbf{r_o}, \mathbf{t})}{B}\right] \cdot \frac{\partial^2 g(\mathbf{r}; \mathbf{r}_o)}{\partial y \partial z_o} \tag{31}$$

with $\mathbf{r} = (x, y, z)$, $\mathbf{r}_o = (x_o, y_o, z_o)$, $dV_o = dx_o dy_o dz_o$ and

$$\frac{\partial^2 g(\mathbf{r}; \mathbf{r}_o)}{\partial y \partial z_o} = \frac{3(y - y_o)}{4\pi}\left[\frac{(z + z_o)}{\left[(x - x_o)^2 + (y - y_o)^2 + (z + z_o)^2\right]^{5/2}} - \frac{(z - z_o)}{\left[(x - x_o)^2 + (y - y_o)^2 + (z - z_o)^2\right]^{5/2}}\right]. \tag{32}$$

Although it is useful to have reduced the problem to "numerical quadrature" (i.e., the volume integral of (31) must be performed numerically once P_c and p_f have been numerically determined), the solution of the Poisson problem (22)–(25) is most rapidly obtained either through finite-difference or finite-element modeling.

[31] Once $\mathbf{u}^{\text{tot}}(\mathbf{r}, t) = \mathbf{u}(\mathbf{r}) + \delta\,\mathbf{u}(\mathbf{r}, t)$ has been determined, we can similarly define the total deviatoric stress tensor as

$$\boldsymbol{\tau}^D_{\text{tot}}(\mathbf{r}, t) = \boldsymbol{\tau}^D(\mathbf{r}) + \delta\boldsymbol{\tau}^D(\mathbf{r}, t) \tag{33}$$

where

$$\delta\boldsymbol{\tau}^D = G\left[\nabla\delta\mathbf{u} + \nabla\delta\mathbf{u}^T - \frac{2}{3}\nabla\cdot\delta\mathbf{u}\,\mathbf{I}\right] \tag{34}$$

are the deviations in the deviatoric stress tensor caused by the fluid-pressure diffusion.

[32] Last, the Coulomb stress τ_{coul} (a scalar) at a point $\mathbf{r}$ on some potential slip surface, having a normal unit vector $\mathbf{n}$ and a tangential unit vector in the direction of potential slip $\hat{\mathbf{t}}$, can then be identified as

$$\tau_{\text{coul}}(\mathbf{r}, \mathbf{n}, \hat{\mathbf{t}}) = \mathbf{n}\cdot\boldsymbol{\tau}^D_{\text{tot}}\cdot\hat{\mathbf{t}} + \mu\left(\mathbf{n}\cdot\boldsymbol{\tau}^D_{\text{tot}}\cdot\mathbf{n} - P_e\right) \tag{35}$$

where μ is the coefficient of friction associated with the slip surface. Positive values of τ_{coul} correspond to an enhanced probability for slip (the Coulomb slip criterion $\tau_{\text{coul}} > 0$ has been met), while negative values correspond to a reduced probability (the criterion has not been met).

4. Numerical Results

[33] As a numerical model, we consider a normal fault dipping at 45°. The rectangular slip surface begins at a depth of $z = 1$ km, and has a down-dip length of 5 km and a parallel-to-surface length of 20 km (see the white dashed box in Figure 4). At $t = 0$, a dislocation displacement of 50 cm is imposed which corresponds to an $M6$ earthquake. The x axis in what follows is taken to be parallel with the fault (and perpendicular to the depth axis z), while the y axis

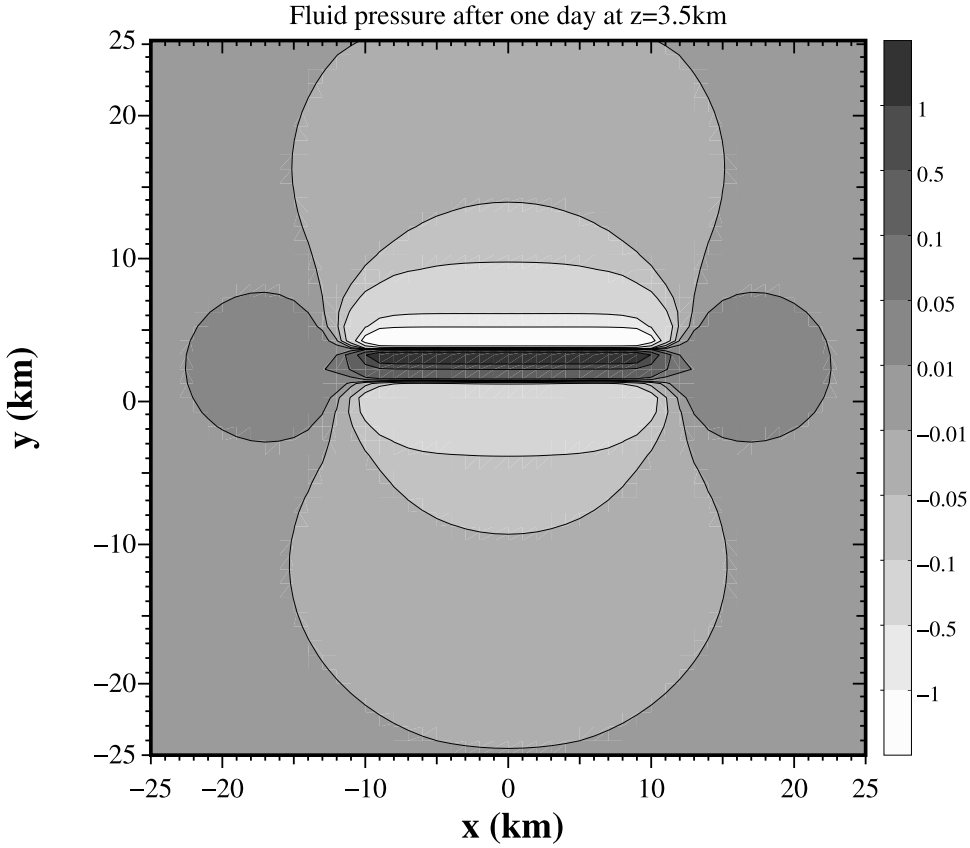

Figure 1. The fluid pressure distribution (MPa) on a horizontal slice through the crust at $z = 3.5$ km one day following the $M6$ earthquake.

extends away from the fault. The *Okada* [1992] program is used to calculate the undrained (instantaneous) stress and strain distribution at $t = 0$. All waves generated during the event are ignored. Given the $P_c(\mathbf{r})$ distribution so determined, the fluid pressure $p_f(\mathbf{r}, t)$ is determined using an explicit time-stepping finite-difference solution of equation (17) (see Gavrilenko (submitted manuscript, 2004) for details of the algorithm). The values used for the various crustal material properties are given in Appendix A.

4.1. Mechanical Response

[34] The fluid-pressure distribution on a horizontal slice through the crust at $z = 3.5$ km and at $t = 1$ day following the slip event is shown in Figure 1. At a point ($x = 0$ km, $y = +2$ km, $z = 3.5$ km) that lies within a compressed region (see Figure 1), the fluid pressure as a function of time is plotted in Figure 2. After roughly 2 years, the fluid pressure at this particular point and for this particular event ultimately returns to zero. However, the principal time constant for the diffusive decay is roughly one month.

[35] As part of our ongoing research program, we plan to numerically solve equations (22)–(25) using finite-difference approximations and determine the Coulomb-stress evolution through time due to fluid-pressure diffusion with the goal of characterizing the temporal nature of aftershock sequences. Our present purpose, however, is to simply demonstrate that the stress tensor evolves through time as the fluid-pressure diffuses. With this goal in mind, we plot in Figure 3a how the total confining pressure $P_c^{\text{tot}}(\mathbf{r}, t) =$

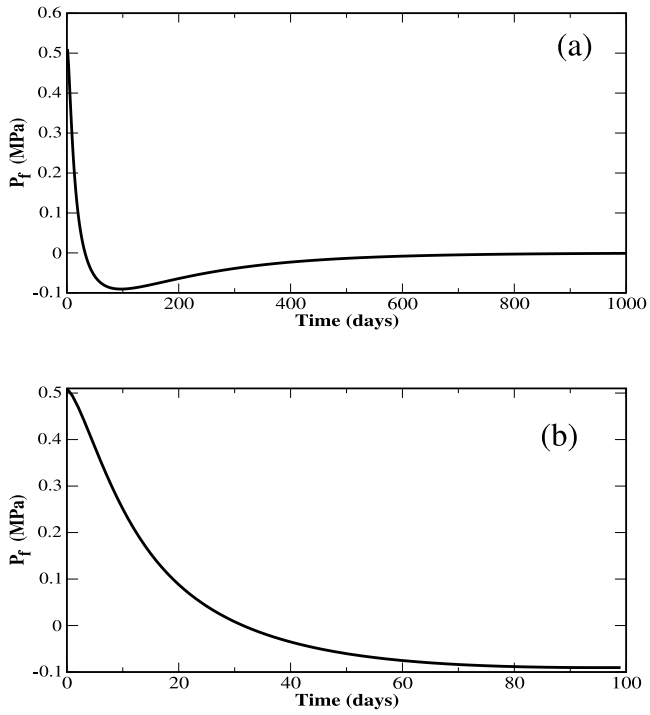

Figure 2. The fluid-pressure variation through time at a point $x = 0$ km, $y = 2$ km and $z = 3.5$ km: (a) response on a time scale of 1000 days, and (b) response on the time scale of 100 days used in the other figures of this article.

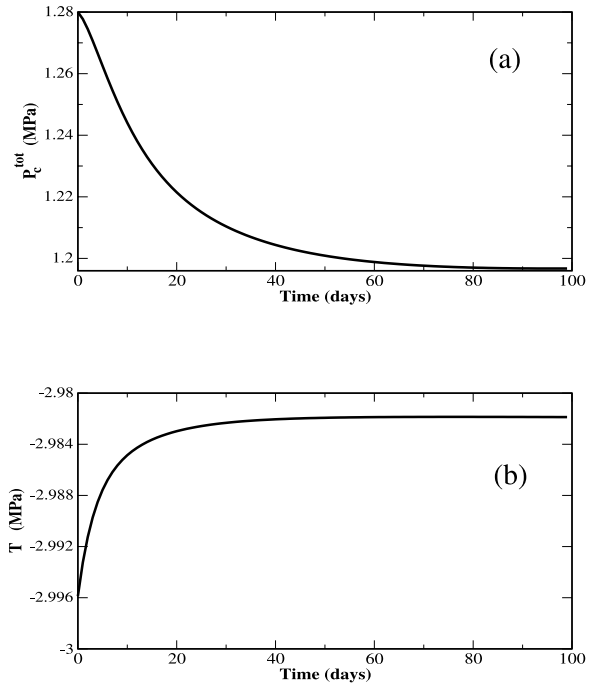

Figure 3. Stress variation through time at the point x = 0 km, y = 2 km, z = 3.5 km: (a) the total confining pressure $P_c^{\text{tot}} = P_c + \delta p_c$ where P_c is the undrained response determined using the program of *Okada* [1992] and δp_c are the fluid-pressure-induced variations determined using equation (19); and (b) the shear-stress proxy T as defined by equation (36).

$P_c(\mathbf{r}) + \delta p_c(\mathbf{r}, t)$ varies through time at the same point (x = 0 km, y = = +2 km, z = 3.5 km) considered above. Equation (19) is used for determining δp_c while the *Okada* [1992] program gives $P_c(\mathbf{r})$.

[36] As a proxy for a typical shear-stress component, we define a stress T as

$$T \equiv G\frac{\partial u_z^{\text{tot}}}{\partial y} = G\frac{\partial u_z(\mathbf{r})}{\partial y} + G\frac{\partial \delta u_z(\mathbf{r}, t)}{\partial y}. \qquad (36)$$

We choose this measure in particular because $\partial \delta u_z(\mathbf{r}, t)/\partial y$ can be determined using equations (31) and (32). The nested integrals over x_o, y_o, and z_o are numerically performed using Simpson's rule [e.g., *Press et al.*, 1992]. Figure 3b is a plot of T through time at the same point (x = 0 km, y = +2 km, z = 3.5 km) already considered.

[37] We see that both the confining pressure and the shear-stress component T are decreasing in amplitude through time due to the fluid pressure diffusion which is the general trend for any point in the crust (i.e., initially negative values become less negative and initially positive values become less positive). The decreasing confining pressure makes the Coulomb stress larger, while the decreasing shear amplitude makes the Coulomb stress smaller. The percent change in P_c is consistently much larger than that in the shear-stress parameter T. The variation in P_c due to diffusion is roughly 1 bar in this example while the variation in T is only 0.1 bars. The amplitude of these changes through time is controlled principally by the dimensionless product αB as equation (19) makes clear. In this example, we have taken α = 0.3 and B = 0.4. However, as discussed earlier, the α and B values appropriate for large samples of faulted crustal rock might be larger with an associated increase in the percent changes of P_c and T.

4.2. Electrical Response

[38] The electric field throughout the uniform crust is given directly by equation (13). Figure 4 is a snapshot of the vertical component E_z on a horizontal slice at z = 500 m and at one day following the earthquake. We choose to plot E_z (rather than a horizontal component) because the horizontal components are zero right on the free surface. Also, the electric field component that is most easily measured in a well is the vertical component. We see that these generated fields have amplitudes of 1 mV/m which are quite large relative to, say, the atmospherically generated diurnal fields which are routinely measured at the μV/m level. Figure 5 gives another snapshot of E_z one day following the earthquake on a vertical slice parallel with the fault at y = +2 km. From equation (13), E_z is directly proportional to the vertical component of the Darcy flow and so these snapshots are also a direct representation of the fluid-flow field.

[39] At the same point (x = 0 km, y = +2 km, z = 3.5 km) already considered, we plot E_z as a function of time in Figure 6. By monitoring the decay of the E field through time, the fluid pressure diffusivity D could, in principle, be deduced at the scale of the initial stress lobes that equilibrate ($\approx$10 km).

5. Conclusions

[40] Fluid equilibration throughout a uniform crust has been modeled in the aftermath of an earthquake. The earthquake was modeled as a normal-fault event with uniform displacement on a predefined rectangular slip surface. The associated undrained stress changes immediately following the earthquake (t = 0) were determined using the *Okada* [1992] numerical program. The subsequent (t > 0) fluid equilibration was modeled using a finite-difference solution of the fluid-pressure diffusion equation (17) subject to open-pore boundary conditions at the surface (p_f = 0 on z = 0). The goal of the paper was to consider how such fluid-pressure equilibration affects both the stress state in the crust and the electric and magnetic fields in the months following an earthquake.

[41] In a uniform crust model, the workhorse relation that allows much about the poroelastic response to be exactly known is equation (15) which quantifies how a mass element changes volume when fluid mass accumulates within it during fluid-pressure diffusion. Using (15) in the poroelastic governing equations allows a simplified determination for how the displacement and stress tensor components throughout the crust are evolving through time (the Poisson boundary-value problem of equations (22)–(25)). The order-of-magnitude amplitude of such fluid-pressure-induced stress changes relative to the t = 0 static stress changes are $O(\alpha B)$. Here, α is the Biot-Willis constant and B is the Skempton coefficient and both properties are

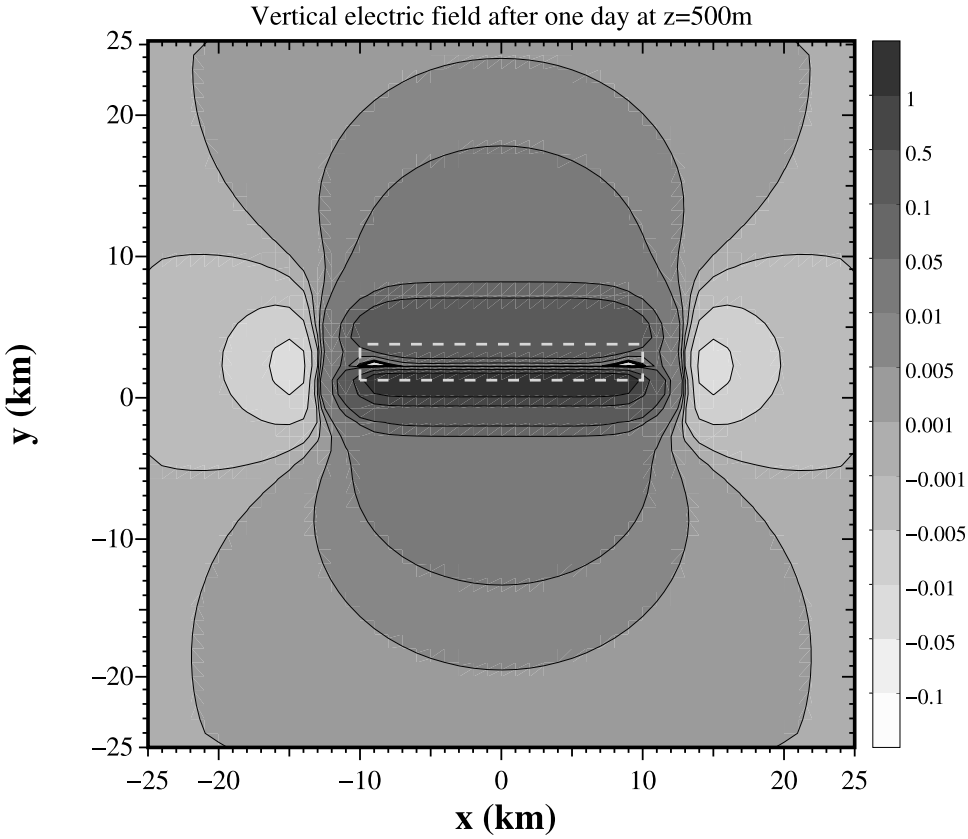

Figure 4. The vertical component of the electric field E_z (mV/m) on a horizontal slice at z = 500 m one day after the earthquake.

typically less than 0.5 for laboratory samples of low-porosity crustal materials. The fluid-pressure-induced changes of the stress-tensor components are thus never huge effects in terms of percent changes; however, they nevertheless can represent bars of Coulomb-stress change for an *M*6 mainshock. Further, it is expected that both α and B will be larger for kilometer-scale samples of a faulted crust; however, we do not speculate on a scaling law for these key parameters here.

[42] As part of our ongoing research agenda, we plan to numerically determine how the Coulomb stress is evolving through time due to fluid-pressure equilibration at all points throughout the crust surrounding the fault with the goal of modeling aftershock sequences. Gavrilenko (submitted manuscript, 2004) has already demonstrated that such aftershock sequences are generally consistent with what is observed; however, he allowed only for the fluid pressure variations of the Coulomb stress without allowing for the stress-tensor variations.

[43] The electric fields in the uniform crust were analytically shown to be exactly proportional to the Darcy fluid flow (equation (13)). No magnetic fields are generated in a uniform crust. The coupling generating the E fields is electrokinetic. A peculiar aspect of the electric field generated in a uniform crust and when open-pore boundary conditions hold at the surface z = 0, is that there is no horizontal component of the electric field along z = 0. However, the vertical component of the electric field is non-zero at the surface and for the *M*6 earthquake model that was numerically treated, it had a maximum amplitude

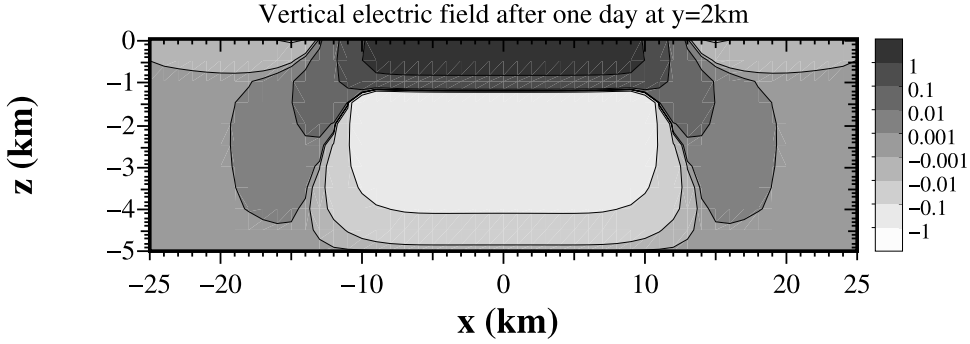

Figure 5. A snapshot of E_z (mV/m) on a vertical slice at y = 2 km one day after the earthquake.

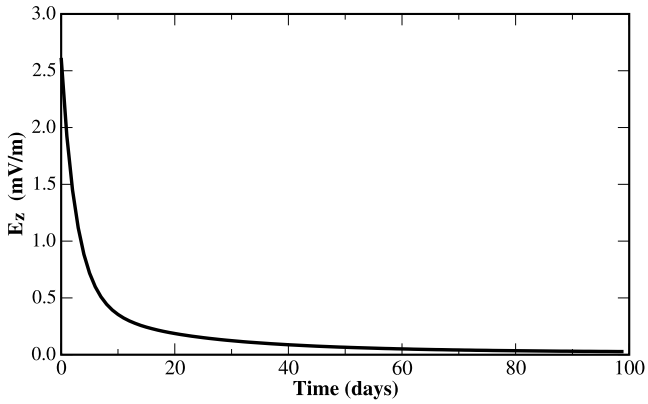

Figure 6. The variation of E_z through time at the point x = 0 km, y = 0 km, z = 500 m.

of roughly 1 mV/m which is large compared to background noise levels.

[44] *Nagao et al.* [2000] have measured the horizontal-component of the electric field at the earth's surface following earthquakes in Japan using dipole electrode pairs. They measure electric fields on the order of 10^{-2} mV/m that turn on after the earthquake and that decay with time constants on the order of minutes to hours. As expected from the present study, such horizontal fields are likely due to localized heterogeneity and associated fluid-pressure diffusion in the local vicinity of the recording stations. It might be interesting to try measuring the electric-potential differences between different points in a monitoring well (vertical component of the E field) or between different wells (horizontal component at depth) as a means of quantifying the Darcy-flow variations through time due to the kilometer-scale diffusion between the stress lobes created after an earthquake. To our knowledge, no such measurements have been published.

Appendix A: Models for the Coefficients

[45] In order to obtain the numerical results, models for the various coefficients need to be established.

[46] To model the poroelastic moduli K_U (undrained bulk modulus) and B (Skempton's coefficient), we assume that the grains are made from a single isotropic mineral having a bulk modulus of K_s = 60 GPa. In this case, the *Gassmann* [1951] and *Biot and Willis* [1957] results are available (the so-called "fluid substitution" relations)

$$B = \frac{1/K_D - 1/K_s}{1/K_D - 1/K_s + \phi\left(1/K_f - 1/K_s\right)} \tag{A1}$$

$$K_U = \frac{K_D}{1 - B(1 - K_D/K_s)} \tag{A2}$$

and where K_D is the drained bulk modulus. Here, K_f = 2.5 GPa is the bulk modulus of the electrolyte saturating the pores. The Biot-Willis constant in this case is simply

$$\alpha = 1 - K_D/K_s \tag{A3}$$

which is indeed seen to be independent of fluid properties.

[47] The remaining moduli that must be specified are K_D and G. Rather than propose models for these drained moduli, we simply use the values of K_D = 45 GPa and G = 30 GPa in the numerical modeling. Furthermore, we take ϕ = 0.01 as the porosity of the uniform crust.

[48] The fluid chemistry is characterized by a salinity M_o (moles/liter) and a pH and affects both the electrokinetic coupling coefficient L and the electrical conductivity σ of the crust. The coupling coefficient L takes the form [cf. *Pride*, 1994]

$$L = -\frac{\epsilon_o \kappa_w}{\eta F}\,\zeta \tag{A4}$$

where $\epsilon_o = 8.85 \times 10^{-12}$ F/m (the permittivity of vacuum) and where κ_f = 80 is the dielectric constant of water which, reasonably, is assumed to be independent of the fluid chemistry (M_o and pH). The fluid viscosity of water is $\eta = 10^{-3}$ Pa s which is also the fluid viscosity to use in the Darcy law. The formation factor F is defined here using *Archie*'s [1942] law

$$F = \phi^{-m} \tag{A5}$$

where m is on the order of 2 for a well-consolidated sandstone, 1.5 for a sand pack, and is closer to 1 for a rock having fracture porosity. In the numerical example, we take m = 1 (and, again, ϕ = 0.01).

[49] The zeta potential ζ quantifies the degree of charge separation in the electric double layer. For pure quartz grains, it can be estimated using the empirical formula [cf. *Pride and Morgan*, 1991]

$$\zeta_{SiO_2}(\text{in Volts}) = (0.01 + 0.025 \log_{10} M_o)\frac{(\text{pH} - 2)}{5} \tag{A6}$$

Though not perfect, this formula captures the major trends of the pH and salinity M_o dependence of the zeta potential of quartz. In rocks, the zeta potential is observed to be smaller in amplitude than for pure quartz. In our simulations, we make the somewhat arbitrary (though consistent with data) choice that $\zeta_{rock} = \zeta_{SiO_2}/3$. The zeta potential at elevated temperatures is typically larger in magnitude than under ambient conditions. In order to make a conservative estimate, this effect is ignored. In the numerical results, we take $M_o = 2.5 \times 10^{-2}$ moles/liter and pH = 7 resulting in $\zeta_{rock} = -10^{-2}$ V which can be considered conservative.

[50] Last, the electrical conductivity σ of the rocks goes as

$$\sigma = \sigma_f / F \tag{A7}$$

where the formation factor is again given by equation (A5). The electrolyte conductivity σ_f is well modeled using the Einstein-Stokes model for ions migrating as spheres of radius R_i through a continuum of water molecules

$$\sigma_f = \frac{e^2}{6\pi\eta}\left(\frac{1}{R_{Na}} + \frac{1}{R_{Cl}}\right) 6.022 \times 10^{26}\, M_o \tag{A8}$$

where $R_{Na} = 1.83 \times 10^{-10}$ m and $R_{Cl} = 1.20 \times 10^{-10}$ m for a NaCl electrolyte, $e = 1.6 \times 10^{-19}$ C is the fundamental

charge, and η is again the fluid viscosity. Using $M_o = 2.5 \times 10^{-2}$ we obtain $\sigma_f = 0.2$ S/m.

[51] The fluid viscosity of the electrolyte is taken to be $\eta = 10^{-3}$ Pa s while the permeability of the crust is assumed to be $k = 10^{-16}$ m^2 (0.1 mD). This k value has been shown by Gavrilenko (submitted manuscript, 2004) to do a reasonable job explaining aftershock sequences. The permeability of the crust at the 10 km scale has never been measured; however, due to the presence of fracture/fault networks, it is known that the permeability increases with scale [e.g., *Gueguen et al.*, 1996; *Gavrilenko and Gueguen*, 1998]. The value of k = 0.1 mD at the 10 km scale is consistent with what is known about such scaling.

[52] **Acknowledgments.** This work was supported by a grant from the French government program ACI "Prévention des Catastrophes Naturelles."

References

Archie, G. E. (1942), The electrical resistivity log as an aid in determining some reservoir characteristics, *Trans. Am. Inst. Min. Metall. Pet. Eng.*, *146*, 54–62.

Bell, M. L., and A. Nur (1978), Strength changes due to reservoir-induced pore pressure and stresses and application to Lake Oroville, *J. Geophys. Res.*, *83*, 4469–4483.

Berge, P. A., H. F. Wang, and B. P. Bonner (1993), Pore-pressure buildup coefficient in synthetic and natural sandstones, *Int. J. Rock Mech. Min. Sci. Geomech. Abstr.*, *30*, 1135–1141.

Biot, M. A. (1956), Theory of propagation of elastic waves in a fluid-saturated porous solid. I. Low-frequency range, *J. Acoust. Soc. Am.*, *28*, 168–178.

Biot, M. A. (1962), Mechanics of deformation and acoustic propagation in porous media, *J. Appl. Phys.*, *33*, 1482–1498.

Biot, M. A., and D. G. Willis (1957), The elastic coefficients of the theory of consolidation, *J. Appl. Mech.*, *24*, 594–601.

Fenoglio, M. A., M. J. S. Johnston, and J. D. Byerlee (1995), Magnetic and electric fields associated with changes in high pore pressure in fault zones: Application to the Loma Prieta ULF emissions, *J. Geophys. Res.*, *100*, 12,951–12,958.

Fitterman, D. V. (1978), Theory of electrokinetic-magnetic anomalies associated with dilatant regions in a layered Earth, *J. Geophys. Res.*, *83*, 5923–5928.

Gassmann, F. (1951), Über die Elastizität poröser Medien, *Vierteljahrsschr. Nat. Ges. Zürich*, *96*, 1–23.

Gavrilenko, P., and Y. Gueguen (1998), Flow in fractured media: A modified renormalization method, *Water Resour. Res.*, *34*, 177–191.

Gueguen, Y., P. Gavrilenko, and M. L. Ravalec (1996), Scales of rock permeability, *Surv. Geophys.*, *17*, 245–263.

Muir-Wood, R., and G. C. P. King (1993), Hydrological signatures of earthquake strain, *J. Geophys. Res.*, *98*, 22,035–22,068.

Nagao, T., Y. Orihara, T. Yamaguchi, I. Takahashi, K. Hattori, Y. Noda, and K. Sayanagi (2000), Co-seismic geoelectric potential changes observed in Japan, *Geophys. Res. Lett.*, *27*, 1535–1538.

Nur, A., and J. R. Booker (1972), Aftershocks caused by pore fluid flow?, *Science*, *175*, 885–887.

Okada, Y. (1992), Internal deformation due to shear and tensile faults in a half-space, *Bull. Seismol. Soc. Am.*, *82*, 1018–1040.

Press, W. H., S. A. Teukolsky, W. T. Vetterling, and B. P. Flannery (1992), *Numerical Recipes*, 2nd ed., Cambridge Univ. Press, New York.

Pride, S. R. (1994), Governing equations for the coupled electromagnetics and acoustics of porous media, *Phys. Rev. B*, *50*, 15,678–15,696.

Pride, S. R. (2004), Relationships between seismic and hydrological properties, in *Hydrogeophysics*, edited by Y. Rubin and S. Hubbard, pp. 217–255, Kluwer Acad., Norwell, Mass.

Pride, S. R., and M. W. Haartsen (1996), Electroseismic wave properties, *J. Acoust. Soc. Am.*, *100*, 1301–1315.

Pride, S. R., and F. D. Morgan (1991), Electrokinetic dissipation induced by seismic waves, *Geophysics*, *56*, 914–925.

Sill, W. R. (1983), Self-potential modeling from primary flows, *Geophysics*, *48*, 76–86.

Skempton, A. W. (1954), The pore-pressure coefficients A and B, *Geotechnique*, *4*, 143–147.

Stein, R. S. (1999), The role of stress transfer in earthquake occurrence, *Nature*, *402*, 605–609.

P. Gavrilenko and F. Moreau, Geosciences Rennes, Universite de Rennes 1, Campus Beaulieu, 35042 Rennes Cedex, France. (gavrilen@univ-rennes1.fr; frederique.moreau@univ-rennes1.fr)

S. R. Pride, Earth Sciences Division, Lawrence Berkeley National Laboratory, 1 Cyclotron Road, MS 90-1116, Berkeley, CA 94729, USA. (srpride@lbl.gov)